J|A|C|S
ARTICLES
Published on Web 03/15/2003

From Weak Interactions to Covalent Bonds: A Continuum in the Complexes of 1,8-Bis(dimethylamino)naphthalene

Paul R. Mallinson,*,† Garry T. Smith,† Chick C. Wilson,‡ Eugeniusz Grech,§ and Krzysztof Wozniak*,||

Contribution from the Chemistry Department, University of Glasgow, G12 8QQ, United Kingdom, ISIS Fascility, Rutherford Appleton Laboratory, Chilton, Didcot, Oxon OX11 0QX, United Kingdom, Technical University of Szczecin, ul. Piastów 42, 71-065 Szczecin, Poland, and Department of Chemistry, University of Warsaw, ul. Pasteura 1, 02-093 Warszawa, Poland

Received November 18, 2002; E-mail: kwozniak@chem.uw.edu.pl

Abstract: Experimental charge density distributions in a series of ionic complexes of 1,8-bis(dimethylamino)-naphthalene **(DMAN)** with four different acids: 1,2,4,5-benzenetetracarboxylic acid (pyromellitic acid), 4,5-dichlorophthalic acid, dicyanoimidazole, and o-benzoic sulfimide dihydrate (saccharin) have been analyzed. Variation of charge density properties and derived local energy densities are investigated, over all inter- and intramolecular interactions present in altogether five complexes of **DMAN**. All the interactions studied {[O···H···O]$^-$, C−H···O, [N−H···N]$^+$, O−H···O, C−H···N, Cπ···Nπ, Cπ···Cπ, C−H···Cl, N−H$^+$ } follow exponential dependences of the electron density, local kinetic and potential energies at the bond critical points on the length of the interaction line. The local potential energy density at the bond critical points has a near-linear relationship to the electron density. There is also a Morse-like dependence of the laplacian of rho on the length of interaction line, which allows a differentiation of ionic and covalent bond characters. The strength of the interactions studied varies systematically with the relative penetration of the critical points into the van der Waals spheres of the donor and acceptor atoms, as well as on the interpenetration of the van der Waals spheres themselves. The strong, charge supported hydrogen bond in the DMANH$^+$ cation in each complex has a multicenter character involving a {[Me$_2$N−H····NMe$_2$]$^+$····X$^{\delta-}$} assembly, where X is the nearest electronegative atom in the crystal lattice.

Introduction

An aromatic diamine 1,8-bis(dimethylamino)naphthalene (**DMAN**) has been known since the early 1940s[1] but its high basicity (pK_a value ca. 12) was first realized by Alder et al.[2] in the late sixties. **DMAN** is the parent molecule of proton sponges[3]—compounds which have attracted considerable interest due to their very high proton affinity, low nucleophilicity, slow protonation/deprotonation, and applications in modeling of enzymatic catalysis processes.[4] One of the primary reasons for their properties is the strain induced by the proximity of the two amine substituents attached in **DMAN** at the peri- positions of the naphthalene rings. With mineral or organic acids proton sponges form very stable ionic complexes containing low barrier intramolecular [N···H···N]$^+$ hydrogen bonding.[3] This H-bonding is asymmetric according to ab initio calculations,[5,6] numerous diffraction studies and isotope shift investigations.[7]

There are already more than 300 papers published on proton sponges and their complexes. Research in this field goes in the following main directions: (a) synthesis of new proton sponges and their complexes;[8−10] (b) mainly theoretical studies of factors responsible for enhanced basicity such as: cationic H-bond energies,[11−13] lone pair−lone pair repulsion energies,[14,15] strain energies,[5,6,16] resonance (aromatic stabilization energies);[13,17] (c)

† Chemistry Department, University of Glasgow.
‡ ISIS Fascility, Rutherford Appleton Laboratory.
§ Technical University of Szczecin.
|| Department of Chemistry, University of Warsaw.

(1) Brown, W. G.; Letang, N., J. *J. Am. Chem. Soc.* **1941**, *63*, 358−361.
(2) Alder, R., W.; Bowman, P. S.; Steele, W. R. S.; Winterman, D., R.; J. *Chem. Soc., Chem. Commun*. **1968**, 723−724.
(3) (a) Staab, H. A.; Saupe, T. *Angew. Chem., Int. Ed. Engl.* **1988**, *27*, 865−879; (b) Alder, R. *Chem. Rev.* **1989**, *89*, 1215−1223; (c) Wozniak, K.; He, H.; Klinowski, J.; Grech, E. *J. Phys. Chem.* **1995**, *99*, 1403−1409; (d) Truter, M. R.; Vickery, B. L. *J. Chem. Soc., Dalton Trans.* **1972**, 395−403; (e) Pyzalska, D.; Pyzalski, R.; Borowiak, T. *J. Crystallogr. Spectrosc. Res.* **1983**, *13*, 211−220; (f) Glowiak, T.; Malarski, Z.; Sobczyk, L.; Grech, E. *J. Mol. Struct.* **1987**, *157*, 329−337; (g) Wozniak, K.; Krygowski, T. M.; Kariuki, B.; Jones, W.; Grech, E. *J. Mol. Struct.* **1990**, *240*, 111−118; (h) Bartoszak, E.; Jaskólski, M.; Grech, E.; Gustafsson, T.; Olovsson, I., *Acta Crystallogr.* **1994**, *B50*, 358−363; (i) Miller, P. K.; Abney, K. D.; Rappe, A. K.; Anderson, O. P.; Strauss, S. H. *Inorg. Chem.* **1988**, *27*, 2255−2261; (j) Brown, D. A.; Clegg, W.; Colquhoun, H. M.; Daniels, J. A.; Stephenson, J. R.; Wade, K. *J. Chem. Soc., Chem. Commun.* **1987**, 889−891; (k) Kanters, J. A.; Schouten, A.; Kroon, J.; Grech, E. *Acta Crystallogr.* **1991**, *C47*, 807−810; (l) Kellett, P. J.; Anderson, O. P.; Strauss, S. H.; Abney, K. D. *Can. J. Chem.* **1989**, *67*, 2023−2029; (m) Woźniak, K.; Wilson, C. C.; Knight, K. S.; Grech, E. *Acta Crystallogr.* **1996**, *B52* 691−696; (n) Woźniak, K.; He, H.; Klinowski, J.; Barr, T. L.; Milart, P. *J. Phys. Chem.* **1996**, *100*, 11 420−11 426; (o) Einspahr, H.; Robert, J.-B.; Marsh, R. E.; Roberts, J. *Acta Crystallogr.* **1973**, *B29*, 1611−1617; (p) Woźniak, K.; He, H.; Klinowski, J.; Nogaj, B.; Lemanski, D.; Hibbs, D.; Hursthouse, M.; Howard, S. *J. Chem. Soc., Faraday Trans.* **1995**, *91*, 3925−3932; (r) Woźniak, K.; He, H.; Klinowski, J.; Jones, W.; Grech, E. *J. Phys. Chem.* **1994**, *98*, 13755−13765; (s) Woźniak, K. *Mol. Struct.* **1996**, *374*, 227−237; (t) Nogaj, B.; Woźniak, K.; Lemanski, D.; Ostafin, M.; Grech, E. *Solid State NMR* **1995**, *4*, 187−191; (u) Woźniak, K.; He, H.; Klinowski, J.; Jones, W.; Barr, T. L. *J. Phys. Chem.* **1995**, *99*, 14667−14677.

experimental studies of structural and spectroscopic properties;[18,19] and finally (d) some applications in catalysis.[4]

A number of new proton sponges such as 1,2,4,5-tetrakis(dimethylamino) benzene, 2,3,6,7-tetrakis (dimethylamino)naphthalene, and other tetrakis(dimethylamino)-naphthalenes have been prepared and structurally determined.[8,9] Also derivatives of acenaphthalene and acenaphthylene, compounds with easily modified basicity, were described in ref 20. Some other new proton sponges include novel cyclam-like macrocyclic tetraamines.[21,22]

A precise additive scheme for describing proton sponge basicity as the sum of proton affinity of an appropriate reference monoamine, the strain released on protonation and the energy of the intramolecular H-bond is described in ref 12.

With respect to enhanced basicity some papers regarding guanidine and cyclopropenimine derivatives have appeared.[23] These compounds have basicities close to Schwesinger's proton sponges.[24−26]

A selective and efficient method for synthesis of fluoroalkyl-(hydrido)complexes of rhodium and iridium has been developed using proton sponges as the hydride source.[12,27] The **DMANH**$^+$ fluoride mixtures appear to be mild and efficient fluorinating reagents.[28,29] Proton sponges can also be used together with $Pd(PPh)_3$ to remove the (2-allyloxy)phenyl group from an organic moiety.[21,30]

The rate of interconversion of different stereoisomers of peri-derivatives has been described in ref 31. Also transition metal complexes with proton sponges have been synthesized and characterized.[32]

Derivatives of 2-methylsparteine, 3-hydroxy-lupanine and 1,2-bis(dialkylaminomethyl) benzene and its complexes with Cu(II) have been studied by kinetic, potentiometric and MS methods.[33]

A possible origin of the high basicity of 2,7-dimethoxy-1,8-bis(dimethylamino)-naphthalene and its possible implications for enzyme catalysis have been studied.[34] The increase of basicity was found to come from the relief of steric repulsion between the dialkylamine groups.

It has been proved for the **DMANH**$^+$ cation[35] that there exists a large $^{2H}J_{NN}$ coupling across the hydrogen bond, mediated by the proton.

The forbidden emission of **DMAN** and of the protonated **DMANH**$^+$ cation lead to a conclusion that ground-state conformers[36,37] exist, differing in the relative arrangement of the dimethylamino groups. In the case of the cation, only one fluorescence band is observed.

DMAN itself and its complexes are very good model systems to study a number of interesting chemical phenomena such as unusual proton affinity, ionic $[N-H\cdots N]^+$ hydrogen bonding and its short- and long-range consequences, aromaticity and conjugation in the aromatic part, and weak hydrogen bonding. Modern high-resolution X-ray diffraction methods allow for a characterization of the nature of chemical interactions.[38,39] We have accomplished our studies by construction of a mathematical model of charge density in a crystal and then by fitting the parameters of such a model to the experimental pattern of diffracted X-rays. We applied the so-called multipole formalism proposed by Hansen and Coppens.[40] In this model, electron density in a crystal is described by a sum of aspherical "pseudoatoms" where the "pseudoatom" density has the form

$$\rho_j(\boldsymbol{r}_j) = \boldsymbol{P}_c\rho_c(r_j) + \boldsymbol{P}_v\kappa'^3\,\rho_v(\kappa'\boldsymbol{r}_j) + \sum_{l=0}^{l_{max}}\kappa''^3\,\boldsymbol{R}_l(\kappa''\boldsymbol{r}_j)\sum_{m=-l_{max}}^{l_{max}}\boldsymbol{P}_{lm\pm}\boldsymbol{d}_{lm\pm}(\vartheta_j,\phi_j)$$

in which the first term describes the core density (P_c stands for the core populations, and ρ_c is the spherically averaged Hartree−Fock core density for the atom). The second term describes the spherical part of the valence density. κ' is an expansion/contraction coefficient which allows the radial density to become more or less diffuse. P_v stands for the valence population. The third term describes the deviation of pseudoatom density from

(4) (a) Gerlt, J. A.; Kreevoy, M. M.; Cleland, W. W.; Frey, P. A. *Chem. Biol.* **1997**, *4*, 259; (b) Cleland, W. W.; Kreevoy, M. M. *Science* **1994**, *264*, 1887; (c) Gerlt, J. A.; Gassman, P. G. *J. Am. Chem. Soc.* **1993**, *115*, 11 552; (d) Frey, P. A. *Science* **1995**, *269*, 104; (e) Cleland, W. W.; Kreevoy, M. M. *Science* **1995**, *269*, 104; (f) Hur, O.; Leja, C.; Dunn, M. F. *Biochemistry* **1996**, *35*, 7378; (g) Ash, E. L.; Sudmeier, J. L.; Fabo, E. C. D.; Bachovchin, W. W. *Science* **1997**, *278*, 1128. (h) Cleland, W. W.; Frey, P. A.; Gerlt, J. A. *J. Biol. Chem.* **1998**, *273*, 25529.
(5) Platts, J. A.; Howard, S. T., Woźniak, K. *J. Org. Chem.* **1994**, *59*, 4647−4651;
(6) Perakylla, M. *J. Org. Chem.* **1996**, *61*, 7420−7425.
(7) Perrin, C. L.; Ohta, B. K. *J. Am. Chem. Soc.* **2001**, *123*, 6520−6526.
(8) Staab, H. A.; Elbl-Weier, K.; Krieger, C. *Eur. J. Org. Chem.* **2000**, 327−333.
(9) Staab, H. A.; Kirsch, A.; Barth, T.; Krieger, C.; Neugebauer, F. A. *Eur. J. Org. Chem.* **2000**, 1617−1622.
(10) Wong, E. H.; Weisman, G. R.; Hill, D. C.; Peed, D. P., Rogers, M. E.; Condon, J. S.; Fagan, M. A.; Calabrese, J. C.; Lam, K.-Ch.; Guzei, I.; Rheingold, A. L. *J. Am. Chem. Soc.* **2000**, *122*, 10 561−10 572.
(11) Ikuta, S. *J. Chem. Phys.* **1987**, *97*, 1900.
(12) Howard, S. T. *J. Am. Chem. Soc.* **2000**, *122*, 8238−8244.
(13) Howard, S. T. *J. Am. Chem.. Soc.* **1996**, *118*, 10 269,
(14) Howard, S. T.; Platts, J. A. *J. Org. Chem.* **1998**, *63*, 3568.
(15) Platts, J. A. *Ph.D. Thesis*, University of Wales, Cardiff, 1996.
(16) Howard, S. T.; Fallis, I. A. *J. Org. Chem.* **1998**, *63*, 7117.
(17) Gobbi, A.; Frenking, G. *J. Am. Chem. Soc.* **1993**, *115*, 2362.
(18) Fox, M. A.; Goeta A. E.; Howard, J. A. K.; Hughes, A. K.; Johnson, A. L.; Keen, D. A.; Wade, K.; Wilson, C. C. *Inorg. Chem.* **2001**, *40*, 173−175.
(19) Bartoszak, E.; Dega-Szafran, Z.; Grunwald-Wyspianska, M.; Jaskólski, M.; Szafran, M. *J. Chem. Soc., Faraday Trans.* **1993**, *89*, 2085−2094.
(20) Ozeryanskii, V. A.; Pozharskii, A. F.; Milgizina, G. R.; Howard, S. T. *J. Org. Chem.* **2000**, *65*, 7707−7709.
(21) Miyahara, Y.; Goto, K.; Inazu, T. *Tetrahedron Lett.* **2001**, *42*, 3097−3099.
(22) Broge, L.; Sotofte, I.; Olsen, C. E.; Springborg, *J. Inorg. Chem.* **2001**, *40*, 3124−3129.
(23) Kovacevic, B.; Maksić, Z. B.; Vianello, R. *J. Chem. Soc., Perkin Trans. 2* **2001**, 886−891.
(24) Schwesinger, R.; Schlemper, H. *Angew. Chem., Int. Ed. Engl.* **1987**, *26*, 1167−1169.
(25) Schwesinger, R.; Misfeldt, M.; Peters, K., von Schnering, H. G. *Angew. Chem., Int. Ed. Engl.*, **1987**, *26*, 1165.
(26) Schwesinger, R.; Schlemper, H.; Hasenfratz, Ch.; Willaredt, J.; Dimbacher, T.; Brener, Th.; Ottaway, C.; Fletschinger, M.; Boele, J.; Fritz, H.; Putzas, D.; Rotter, H. W.; Bordwell, F. G.; Satish, A. V.; Ji, G. Z.; Peters, E.-M.; von Schnering, H. G. *Liebigs Ann. Chem.* **1996**, 1055.
(27) Hughes, R. P.; Kovacik, I.; Lindner, D. C.; Smith, J. M.; Willemsen, S.; Zhang, D.; Guzei, I. A.; Rheingold A. L. *Organometallics* **2001**, *20* (14), 3190−3197.]
(28) Darabantu, M.; Lequeux, T.; Pommelet, J.-C.; Ple, N.; Turck, A.; Toupet, L. *Tetrahedron Lett.* **2000**, *41*, 6763−6767.
(29) Darabantu, M.; Lequeux, T.; Pommelet, J.-C.; Ple, N.; Turck, A. *Tetrahedron* **2001**, *57*, 739−750.
(30) Arranz, E.; Boons, G.-J. *Tetrahedron Lett.* **2001**, *42*, 6469−6471.
(31) Lloyd-Jones, G. C. *Synlett.* **2001**, *2*, 161−183.
(32) Wustefeld, H.-U.; Kaska, W. C.; Schuth, F.; Stucky, G. D.; Bu, X.; Krebs, B. *Angew. Chem., Int. Ed. Engl.* **2001**, *40*, 17].
(33) Schroeder, G.; Boczon W.; Łeska, B.; Eitner, K.; Kozioł, B.; Brzezinski, B. *J. Mol. Struct.* **2001**, *597*, 93−100.
(34) Gua, H.; Salahub, D. R. *J. Mol. Struct. (THEOCHEM)* **2001**, *547*, 113−118.
(35) Pietrzak, M.; Wehling, J.; Limbach, H.-H.; Golubiev, N. S.; Lopez, C.; Claramount, R. M.; Elguero, J. *J. Am. Chem. Soc.* **2001**, *123*, 4338−4339.
(36) Szemik-Hojniak, A.; Rettig, W.; Deperasińska, I. *Chem. Phys. Lett.* **2001**, *343*, 404−412.
(37) Szemik-Chojniak, A.; Zwier, J. M.; Buma, W. J.; Bursi, R.; van der Waals, J. H. *J. Am. Chem. Soc.* **1998**, *120*, 4840.
(38) Coppens, P. X-ray Charge Densities and Chemical Bonding, Oxford University Press: Oxford, 1997.
(39) Koritsanszky, T. S.; Coppens, P. *Chem. Rev.* **2001**, *101* (6), 1583−1621.
(40) Hansen, N. K., Coppens, P. *Acta Cryst.* **1978**, *A34*, 909.

sphericity. This is represented by deformation functions taking the shape of density normalized spherical harmonics $d_{lm}\pm$ of order l oriented with index m. The radial term for the deformation functions takes the form of normalized Slater (or Gaussian) functions $R_l(\kappa'' r_j)$ with an expansion-contraction parameter κ''.

The continuous electron density in the crystal is then modeled as a sum of atom centered charge distributions

$$\rho(r) = \sum_j \rho_j(r_j)$$

Once the experimental electron density has been established, Bader's "Atoms-in-Molecules approach"[41,42] provides an excellent tool for the interpretation of X-ray determined charge densities. An informative analysis of both the theoretical and experimental charge density is based upon the topological properties of the density $\rho(\mathbf{r})$. Any bonded pair of atoms has a bond path, i.e., a line of the highest electron density linking them. The point on this line where the gradient of ρ, $\nabla\rho(\mathbf{r})$, is equal to zero, is termed the bond critical point (BCP) and the properties of the density at this point, ρ_b, give quantitative information on that bond's characteristics. A bond path between a pair of noncovalently bonded atoms is called an interaction line. Its length, which can be different from the length of the internuclear vector, will be denoted as R_{ij}. In our opinion, R_{ij} better represents the influence of the local electronic environment on a given interaction.

The laplacian of the density ($\nabla^2\rho(\mathbf{r})$) contains a large amount of chemical information. Because this is the second derivative of the electron density, it indicates where the density is locally concentrated ($\nabla^2\rho(\mathbf{r}) < 0$) and depleted ($\nabla^2\rho(\mathbf{r}) > 0$) and, hence, graphically shows features such as bonds and lone pairs, which are not observable in $\rho(\mathbf{r})$ itself. Ellipticities at BCPs are defined in terms of the ratio of the curvatures of ρ_b in directions normal to the bond, and represent the deviations of the bonding density from cylindrical symmetry. The topology of the charge distributions in a molecule can be represented as a map of the bond paths and interaction lines connecting atomic nuclear positions, called a molecular graph.

Koch and Popelier[43] have utilized Bader's AIM theory to produce specific criteria to characterize weak interactions and, thus, classify hydrogen bonds in particular. They provide eight necessary criteria to allow the conclusion that hydrogen bonding is present in a particular case. The first four criteria can be summarized as follows:

(1) Topology. Bond critical points should be found between the donor hydrogen atom and the acceptor atom of the hydrogen bond, and these two atoms should be linked by a bond path.

(2) Charge Density at the BCP. A relationship should exist between ρ_b and overall hydrogen bond energy.

(3) Laplacian of the Charge Density at BCP. This value should be positive, i.e., typical of the ionic type of interactions, and within a sensible range. The calculated values for $\nabla^2\rho_b$ also correlate with the interaction energy.

(4) Mutual Penetration of the Hydrogen and Acceptor Atoms. This criterion compares the nonbonded radius of the donor (r_D°) and acceptor (r_A°) atoms, with their corresponding bonding radii (r_D and r_A). The nonbonding radius is taken to be the distance from the nucleus to an arbitrary charge density contour, taken at 0.001 au in this case, equivalent to the gas-phase van der Waals radius of the atom. The bonding radius is taken to be the distance from the nucleus to the BCP. This definition allows an easy separation of the penetrations from each of the two atoms involved. The difference Δr is taken as the nonbonding minus the bonding radius ($r^\circ - r$).

In a hydrogen bond, the hydrogen atom should be more penetrated than the acceptor atom, (i.e., $\Delta r_D > \Delta r_A$). Further, a positive interpenetration, and thus positive value of $\Delta r_D + \Delta r_A$, is necessary to characterize an interaction as a hydrogen bond, as opposed to merely a van der Waals interaction. The authors assertion is that out of all the others, these criteria [$\Delta r_D - \Delta r_A > 0$ and $\Delta r_D + \Delta r_A > 0$] alone are *necessary and sufficient* to prove the presence of a hydrogen bond. They also provide four additional necessary criteria that are much more expensive to calculate since they require integration over atomic basins: loss of charge of the hydrogen atom, destabilization of the hydrogen atom, decrease of the dipolar depolarization of the hydrogen atom, and decrease in hydrogen atom volume.

In this work, we follow up our earlier studies of **DMAN**[44] and its complex with dichloromaleic acid[45] and experimentally verify the approach of Koch and Popelier[43] in the characterization of weak interactions in a series of **DMAN** complexes. We examine (a) different types of interesting weak interactions such as C−H···Acceptor (O, N, Cl) and strong ionic $[N-H\cdots N]^+$, $[O\cdots H\cdots O]^-$ hydrogen bonds, $\pi\cdots\pi$ interactions, and possible C···N attractive interactions; (b) the role of a minor secondary $[Me_2N-H\cdots NMe_2]^+\cdots X^{\delta-}$ interaction of the $[Me_2N-H\cdots NMe_2]^+$ fragment with the nearest electronegative atom ($X^{\delta-}$) in the crystal.

This work also follows up extensive studies by Espinosa et al. on the topological and energetic properties of the electron density distributions in hydrogen-bonded systems.[46−51] They make use of 83 published charge density experiments on compounds with X−H···O (X = C, N, O) hydrogen bonds. For example, they found for closed-shell interactions, a close fit of the local kinetic and potential energy densities at hydrogen-bond critical points to an exponential function,[46] and a number of relations between kinetic and potential energy densities and Hessian eigenvalues.[47,48] They have also shown that the interaction potential can be derived from the total energy density, and that it follows well-defined functional forms, such as Morse, Buckingham, or Matsuoka−Clementi−Yoshimin.[49] In two recent papers based on quantum-mechanical calculations for X−H···F hydrogen bonds, they find a similar functional form for the variation of laplacian at crtical points with H···F

(41) Bader, R. F. W. *J. Phys. Chem.* **1998**, *A102*, 7314−7323.
(42) Bader, R. F. W. Atoms in Molecules: A Quantum Theory; Oxford University Press: Oxford, U.K. 1990.
(43) Koch, U.; P. L. Popelier, *J. Phys. Chem*. **1995**. *99*, 9747−9754.
(44) Mallinson, P. R.; Woźniak, K.; Wilson, C. C.; McCormac, K. L. Yufit, D. S. *J. Am. Chem. Soc.* **1999**, *121*, 4640−4646.
(45) Mallinson, P. R.; Woźniak, K.; Smith, G. T.; McCormac, K. L. *J. Am. Chem. Soc.* **1997**, *119*, 11 502−11 509.
(46) Espinosa, E.; Molins, E.; Lecomte, C. *Chem. Phys. Lett.* **1998**, *285*, 170−173.
(47) Espinosa, E.; Lecomte, C.; Molins, E. *Chem. Phys. Lett.* **1999**, *300*, 745−748.
(48) Espinosa, E.; Souhassou, M.; Lachekar, H.; Lecomte, C. *Acta Crystallogr*. **1999**, *B55*, 563−572.
(49) Espinosa, E.; Molins, E. *J. Chem. Phys.* **2000**, *113*, 5686−5694.
(50) Espinosa, E.; Alkorta, I.; Rozas, I.; Elguero, J.; Molins, *Chem. Phys. Lett.* **2001**, *336*, 457−461.
(51) Espinosa, E.; Alkorta, I.; Elguero, J.; Molins, *J. Chem. Phys.* **2002**, *117*, 5529−5542.

Scheme 1

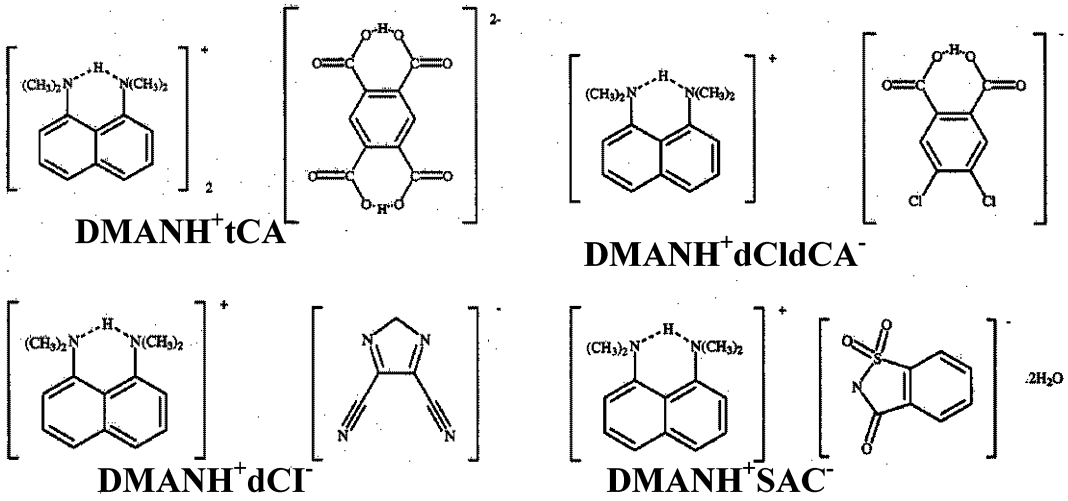

distance.[50,51] Here, we aim to apply these types of analyses to the DMAN complexes.

The whole series of compounds we have studied includes the ionic complexes of protonated **DMAN** with the anions (shown in Scheme 1) of the following acids: 1,2,4,5-benzenetetracarboxylic acid (pyromellitic acid), 4,5-dichlorophthalic acid, dicyanoimidazole, and o-benzoic sulfimide dihydrate (saccharin). The names of the complexes are hereafter abbreviated as **DMANH**$^+$**tCA**$^-$, **DMANH**$^+$**dCldCA**$^-$, **DMANH**$^+$**dCI**$^-$, and **DMANH**$^+$**SAC**$^-$. The labeling schemes of the atoms and the ORTEP illustration of their thermal motions are shown in Figure 1. We shall in addition draw on our previously published results for the complex of DMAN with dichloromaleic acid.[45]

The reasons for small structural changes of the **DMANH**$^+$ cation include possible minor interactions of the H-bonded fragment with the nearest counterion in the crystal lattice. By variation of the anions we will generate variation of minor components in the hydrogen bonding in **DMANH**$^+$ complexes. Ideally, this will be reflected in details of the electron density distributions.

Experimental Section

Crystals of the compounds studied are well-defined colorless prisms, grown by slow evaporation from acetonitrile. Single-crystal, high-resolution, low-temperature X-ray diffraction data for the **DMAN** complexes were collected using a Brucker−Nonius kappa CCD diffractometer and Oxford Cryosystems low-temperature attachment. Data reduction and empirical absorption corrections were carried out with the *DENZO* and *SORTAV*[52] programs. The high-resolution X-ray diffraction experiments are supplemented by the use of neutron diffraction data. Neutrons are an excellent probe for studying both the structure and dynamics of the condensed state.[53] The purpose of the neutron part of this work is to determine as precisely as possible the positions of atoms, in particular hydrogen atoms, and their thermal parameters in complexes of **DMAN**.

Neutron Diffraction Data Collection and Refinement. Neutron measurements were made using the time-of-flight Laue diffraction technique at a temperature of 100 K, the same temperature as used in the X-ray experiment. The procedure used was similar to that described in refs 44 and 45. The crystal data and a summary of the X-ray and neutron data collections and refinements are shown in Table 1.

Multipole Refinement. The program XDLSM (described in an earlier paper[45]) of the package XD[54] was used for the multipole refinement. Anisotropic temperature factors were applied to describe the thermal motion of all atoms. Scattering factors for all atoms were derived from wave functions tabulated by Clementi and Roetti.[55] The multipole expansion was truncated at the octapole level for carbon, oxygen and nitrogen atoms, and at the dipole or quadrupole level for hydrogen atoms. Because all atoms are in general positions, the space group symmetry places no restrictions on the allowed multipole functions. Separate κ', κ'' were employed for chemically different groups of atoms. Their values were allowed to vary, except those relating to H and κ'' for C, N, O, which were fixed at theoretically derived values.[56] Coordinates and anisotropic displacement parameters for the hydrogen atoms only, were fixed at the values obtained from neutron diffraction experiments. We found no systematic difference between the displacement parameters for the non-hydrogen atoms obtained by X-ray and neutron diffraction. It was therefore not necessary to apply any correction to the parameters of the hydrogen atoms.[57]

Results and Discussion

Details of the unit cell parameters, final R-factors, goodness of fit, and the ranges of residual density over the whole asymmetric units and other details of the refinements for the **DMANH**$^+$ complexes shown in Scheme 1 are given in Table

(52) Blessing, R. H. *J. Appl. Crystallogr.* **1989**, *22*, 396−397; Blessing, R. H. *Acta Crystallogr., Sect. A* **1995**, *51*, 33−38.
(53) (a) Wilson, C. C. *Single-Crystal Neutron Diffraction From Molecular Materials*, World Scientific Publishing Co., London, 2000; (b) Willis, B. T. M. *Thermal Neutron Diffraction*; Oxford University Press: Oxford, U.K., 1970. (c) Windsor, C. G., *Pulsed Neutron Scattering*, Taylor&Francis Ltd., London, U.K., 1981. (d)Bacon, G. E., *Neutron Diffraction*, Clarendon Press: Oxford, U.K. 1975.
(54) Koritsanszky, T. S.; Howard, S.; Richter, T.; Mallinson, P. R.; Su, Z.; Hansen, N. K., XD, a computer program package for multipole refinement and analysis of charge densities from X-ray diffraction data. Free University of Berlin, Germany; University of Wales, Cardiff, UK.; University of Glasgow, U.K.; University of Buffalo, USA.; University of Nancy, France, 1995.
(55) Clementi, E.; Roetti, C. *Atomic Data and Nuclear Data Tables* **1974**, *14*, 177−478.
(56) Volkov, A.; Abramov, Y. A.; Coppens, P. *Acta Cryst.* **2001**, *A57*, 272−282.
(57) Blessing, R. H. *Acta Crystallogr.* **1995**, *A51*, 33−38.

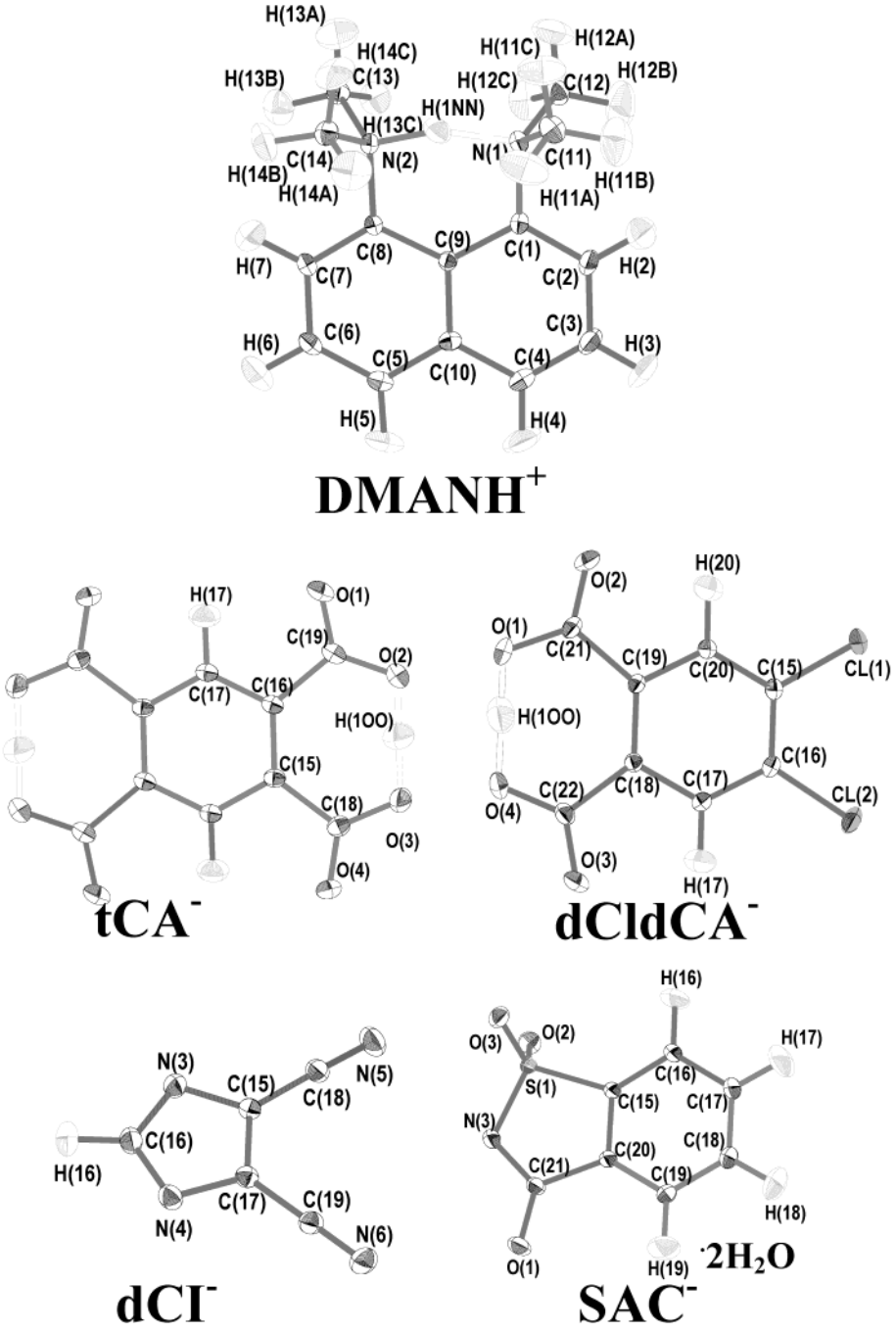

Figure 1. Numbering schemes and atomic displacement parameters (ADPs) for the ionic complexes of **DMANH**$^+$ cation with **tCA**$^-$, **dCldCA**$^-$, **dCI**$^-$, and **SAC**$^-$ obtained for hydrogen atoms from neutron data at 100 K. The ellipsoids are drawn at the 50% probability level.

1. Almost all bonds pass Hirschfeld's rigid bond test.[58] The largest $\Delta_{A,B}$ values are 0.0014 Å^2 for O(4)−C(18) in **DMANH**$^+$**tCA**$^-$, 0.0012 Å^2 for Cl(2)−C(16) and 0.0011 Å^2 for N(2)−C(13) in **DMANH**$^+$**dCldCA**$^-$.

The hydrogen atoms in the covalent N(2)−H(1NN) bond carry a positive charge in the range 0.32e to 0.39e (see the Supporting Information), whereas the aromatic and aliphatic hydrogen charges are close to zero within the level of errors. The same is true for the aromatic carbon atoms. However, for the methyl carbons in all except the saccharide complex a significant positive charge is found (ca. 0.4e).

There seems not to be a significant difference between the charges of the donor and acceptor nitrogen atoms. They are in the range from −0.18(2)e to −0.41(2)e. All of the charges are obtained from the multipole refinement. As one can see from Figure 2, the proton in the [N−H···N]$^+$ hydrogen bridge is very sensitive to local interactions. The electron density associated with this proton is shared with the two nitrogens in the **DMANH**$^+$ complex with **tCA**$^-$ anion, and is separated from the valence shell charge concentration of the acceptor N(1) atoms in the other three complexes. In all of the cations, there is a noticeable polarization of the lone electron pair of the acceptor N(1) atom as previously observed in the dichloromaleic acid complex of **DMAN**.[45]

(58) Hirschfeld, F. L. *Acta Crystallogr.* **1976**, *A32*, 239−244.

Table 1. Experimental X-ray and Neutron Data

compd formula	DMANH$^+$tCA$^-$ $2C_{14}H_{18}N_2 \cdot C_{10}H_6O_8$	DMANH$^+$dCl$^-$ $C_{14}H_{18}N_2 \cdot C_5H_2N_4$	DMANH$^+$dCldCA$^-$ $C_{14}H_{18}N_2 \cdot C_8H_4O_4Cl_2$	DMANH$^+$SAC$^-$ $C_{14}H_{18}N_2 \cdot C_7H_5NSO_3 \cdot 2H_2O$
formula weight	682.8	332.4	449.3	433.52
space group	*Pbca* (orthorhombic)	*Pbca* (orthorhombic)	$P\bar{1}$ (triclinic)	$P2_1/n$ (monoclinic)
temperature/K	100(5)	100(5)	100(5)	100(5)
unit cell dimensions/Å				
a	15.489(1)	15.052(1)	9.252(1)	9.252(1)
b	12.509(1)	14.069(1)	9.567(1)	9.169(1)
c	17.581(1)	16.326(1)	12.972(1)	24.933(1)
α/°			75.09(1)	
β/°			71.26(1)	95.77(1)
γ/°			70.68(1)	
V/Å^3	3406.4(4)	3457.2(4)	1011.3(2)	2104.4(3)
Z	4	8	2	4
D_c/g cm^{-1}	1.331	1.277	1.475	1.368
F(000)	1448	1408	468	920
absorption coefficient/mm^{-1}	0.09	0.08	0.35	0.18
radiation	MoK$_\alpha$ $\lambda = 0.7107$ Å	MoK$_\alpha$	MoK$_\alpha$	MoK$_\alpha$
$(\sin\theta/\lambda)$max/Å^{-1}	0.999	1.000	1.081	1.002
no. of symmetry - independent reflections	14182	14476	16626	17448
refined on	F^2	F^2	F^2	F^2
$R(F)$	0.045	0.048	0.050	0.036
$R_w(F)$	0.021	0.022	0.019	0.027
S	1.85	1.91	2.35	1.59
N_{obs}/N_{ear}	17.3	1.7.9	19.3	20.0
weighting scheme	$w = (1/\sigma^2(F) = (4/F^2/\sigma^2(F^2)$	$w = (1/\sigma^2(F) = (4/F^2/\sigma^2(F^2)$	$w = (1/\sigma^2(F) = (4/F^2/\sigma^2(F^2)$	$w = (1/\sigma^2(F) = (4/F^2/\sigma^2(F^2)$
$\sigma^2(F^2) = \sigma^2_{counting}$ $(F^2) + P^2F^4$, $P = 0.01$				
positional and thermal parameters for H atoms taken from neutron diffraction				
range of residual density in asymmetric unit/eÅ^{-3}	−0.24 − 0.26	−0.23 − 0.24	−0.29 − 0.32	−0.35 − 0.28
neutron data collection method and site	time of flight Laue diffraction, instrument SXD ISIS pulsed neutron sources (RAL, UK)	SXD	SXD	SXD
neutron wavelength	0.5 - 5Å	0.5 - 5Å	0.5 - 5Å	0.5 - 5Å
temperature/K	100	100	100	100
crystal dimensions/mm	5 × 5 × 2	5 × 5 × 5	5 × 5 × 5	5 × 5 × 5
θ range for neutron data collection	1.4 - 46°	1.4 - 46°	1.4 - 46°	1.4 - 46°
$(\sin\theta/\lambda)$max/Å^{-1} for $\lambda = 0.7107$Å	1.02	1.13	1.24	1.18
no. of symmetry independent reflections	2266	3275	5694	3758
refined on	F^2	F^2	F^2	F^2
$R(F)$	0.086	0.078	0.071	0.092
$R_w(F)$	0.061	0.060	0.067	0.077
S	5.1	6.7	4.5	5.9
N_{obs}/N_{ear}	5.5	8.1	12.1	7.3

In two of the anions (**tCA**$^-$ and **dCldCA**$^-$) there are strong, linear ionic [O···H···O]$^-$ hydrogen bonds (see Figure 3). The H(1OO) protons participating in those bonds carry positive charges 0.27(1)e and 0.30(1)e, respectively. Similarly, as in the case of the dichloromaleic complex, their valence shell charge concentrations are separated from the donor and acceptor oxygen atoms.

In general, the **DMANH**$^+$ cation in all four complexes is almost planar. However there are significant differences in the structural parameters between the left and right parts of the moiety. The largest differences occur for the CN bonds and C(1) and C(8) ipso angles (Figure 4a and 4b). For the C(8)−N(2) and C(1)−N(1) bonds, the average lengths are 1.4637 Å and 1.4566 Å, respectively. The respective averaged C(1), C(8) ipso angles are 121.01° and 121.61°. These structural parameters reflect the consequences of the asymmetry of the [N(2)−H(1NN)···N(1)]$^+$ H-bonding. This asymmetry is transmitted over the nearest fragments of the cation and also to the other part of the molecule [C(3)−C(4), C(5)−C(6) bonds]. There are also significant differences between the four complexes with respect to the geometry of the **DMANH**$^+$ cation. Furthermore, for all four complexes, there is a variation of bond lengths in the naphthalene moiety characteristic of aromatic systems with C(1)−C(2), C(3)−C(4), C(5)−C(6), and C(7)−C(8) significantly shorter than the other aromatic bonds. This can be attributed to the different interactions involving the cations.

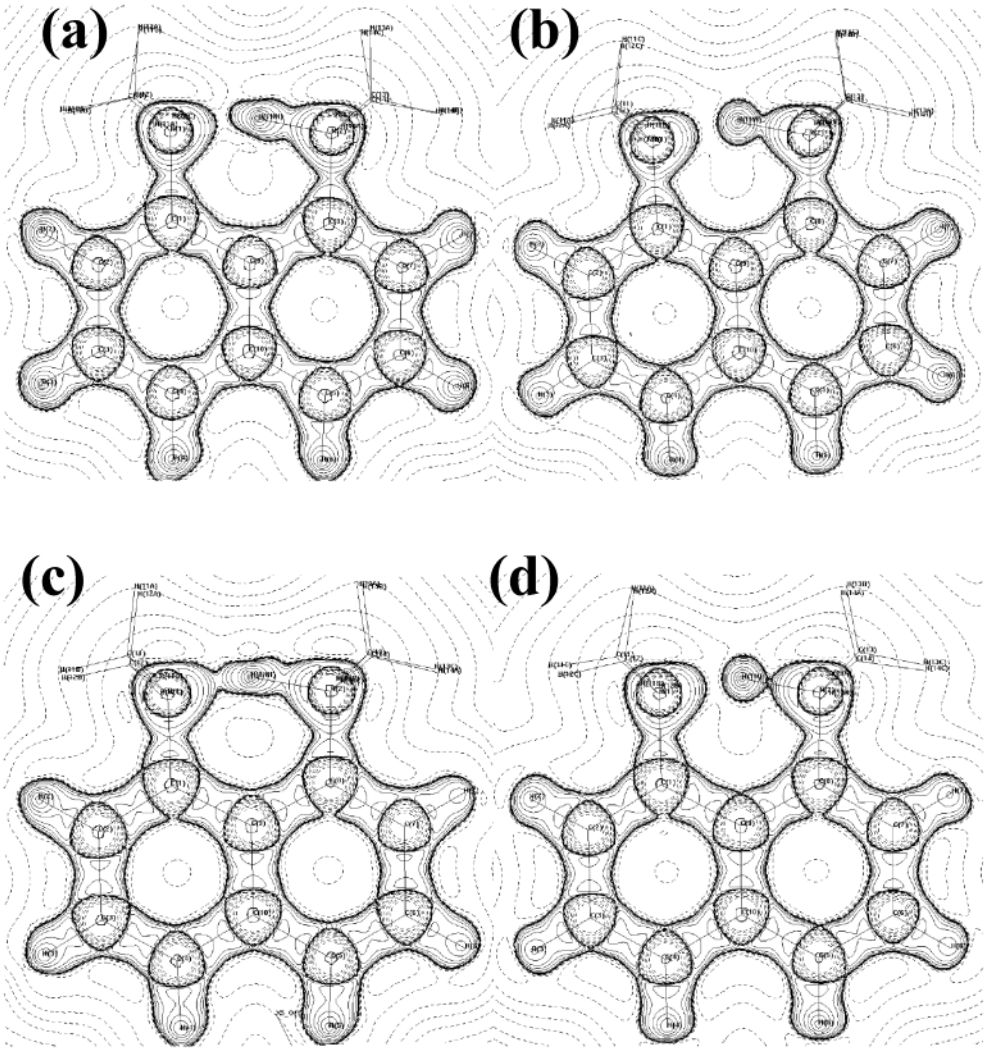

Figure 2. Valence shell concentration and depletion of electron density in **DMANH**$^+$ cations taken from (a) **dCI**$^-$, (b) **dCldCA**$^-$, (c) **tCA**$^-$, and (d) **SAC**$^-$.

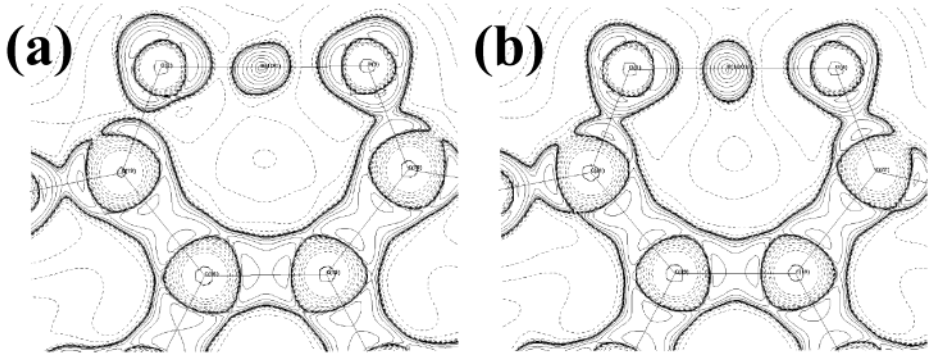

Figure 3. Valence shell charge concentrations in truly ionic [O···H···O]$^-$ hydrogen bonds in: (a) **tCA**$^-$ and (b) **dCldCA**$^-$.

When the geometry of the **DMAN** base[44] is compared with the geometries of the **DMANH**$^+$ cation one can estimate the consequences of protonation and H-bond formation in the cation. We would only mention further that on protonation of **DMAN** the entire cation becomes more planar than the **DMAN** molecule. Other significant structural changes in the cation under protonation are the following: (i) the lengthening of the CN bonds, (ii) the increase of the C(1) and C(8) ipso angles, and the decrease of the N−C−C(9) angles, (iii) the shortening of the C(3)−C(4), and C(5)−C(6) bond lengths.

Properties of the Charge Distribution. The values of ρ_b are shown in Figure 4c. There is a consistency in the four **DMANH**$^+$ cations as regards the topological properties of the charge distributions. For example, for the bonds C(8)−N(2) and

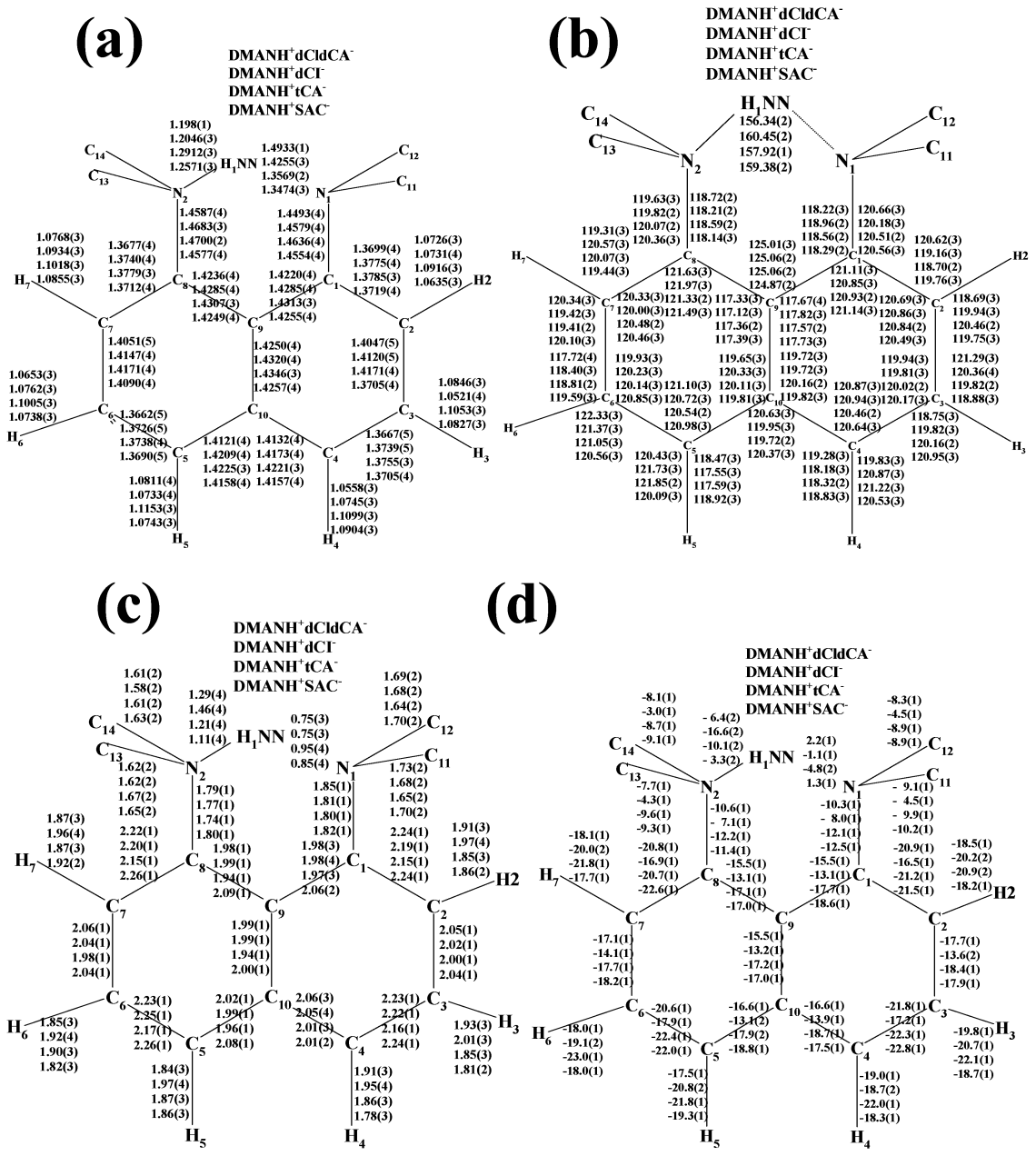

Figure 4. Geometry of the **DMANH**$^+$ cation: (a) bond lengths [Å], (b) valence angles [°], and selected properties at BCPs: (c) ρ_b [eÅ^{-3}], and (d) $\nabla^2\rho_b$ [eÅ^{-5}].

C(1)−N(1), ρ_b reflects the difference in the CN bond lengths resulting from asymmetric protonation (on average 1.78 eÅ^{-3} and 1.82 eÅ^{-3}, respectively). There is also a clear difference in the values of ρ_b between the covalent and H-bonded NH bonds: on average 1.27 eÅ^{-3} and 0.83 eÅ^{-3} for N(2)−H(1NN) and H(1NN)...N(1), respectively. Furthermore, the aromatic CC bonds show the same systematic variation in ρ_b as previously noted for the bond lengths, the shorter CC bond lengths being associated with the larger values of ρ_b.

An unexpected result is found in the context of the covalent bonds in the dimethylamino- groups. The ρ_b values in the C−H bonds are consistently larger than those in the C−N bonds for both of the dimethylamino groups in all four complexes, with an average difference in ρ_b values in these two classes of bonds ca. 0.3 eÅ^{-3}.

The distribution of laplacian for all four complexes is shown in Figure 4d. Within experimental error **DMANH**$^+$ is symmetrical with respect to $\nabla^2\rho_b$ across the line passing through the central C(9)−C(10) bond. In general, there is a tendency for the variation in lengths characteristic of aromatic CC bonds to be reflected in the laplacian values at the BCPs.

The values of ellipticities (see the Supporting Information), as expected, tend to be higher for the aromatic CC bonds (in the range 0.09 to 0.25) than for single C−N and C−H bonds (ellipticity close to zero).

Characterization of Weak Interactions. This study is focused on Koch and Popelier's[43] first four criteria. The table containing all the parameters characterizing 63 interactions present in the four **DMAN** complexes studied in this work and one published earlier[45] is in the Supporting Information. The

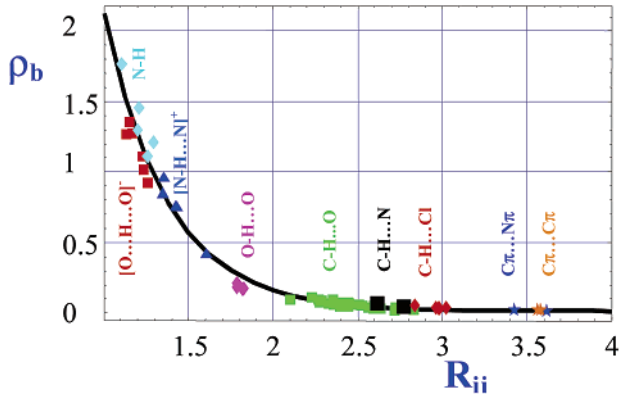

Figure 5. Exponential dependence of ρ_b [eÅ^{-3}] on the bond path length R_{ij} [Å] for H···X: $\rho_b = 0.01(1) + \exp[3.4(2) - 2.7(2)R_{ij}]$, curvilinear correlation coefficient $R = 0.99$ for $N = 63$ data points.

interactions range in type from weak $\pi\cdots\pi$ interactions to covalent bonds. We now review the compliance of our data with the criteria.

Bond critical points and linking bond paths are found between the donor and acceptor atoms for all interactions. Additionally, we analyzed the variation of ρ_b as a function of the length of interaction line (Figure 5).

All these interactions follow an exponential dependence although different types of interactions tend to occupy particular sub-ranges of R_{ij}. This dependence is analogous to Pauling's relation between bond order and internuclear distances.[45,48,51,59] For the smallest R_{ij} values (less than 1.3 Å) ρ_b has values characteristic of covalent bonds (Figure 5). These are [O−H···O]$^-$, [N−H···N]$^+$, and N−H$^+$. Then in the intermediary range of R_{ij} (from 1.3 to 2.1 Å) the electron density at BCP drops significantly to ~0.15eÅ^{-3}—these include O−H...O interactions which are hydrogen bonds involving water molecules. Above $R_{ij} = 2.1$ Å the weakest types of interactions (C−H···O, C−H···Cl, C−H···N, C$\pi\cdots$Nπ, and C$\pi\cdots$Cπ) are represented with ρ_b less than 0.1 eÅ^{-3}.

It is possible to relate the charge density parameters at the donor...acceptor critical points to local energy densities according to the following equations[60,42]

$$G(r_{CP}) = \frac{3}{10}(3\pi^2)^{2/3}\rho^{5/3}(r_{CP}) + \frac{1}{6}\nabla^2\rho(r_{CP})$$

where $G(r_{CP})$ is the local electronic kinetic energy density, ρ and ∇^2 are the electron density and laplacian at the CP, and

$$V(r_{CP}) = \frac{1}{4}\nabla^2\rho(r_{CP}) - 2G(r_{CP})$$

where V stands for the local potential energy density. All quantities are in atomic units. $G(r_{CP})$, the local electronic kinetic energy density, is said to reflect the Pauli principle,[46] whereas the local potential energy density is interpreted as a kind of a pressure of nuclei on electrons interacting at CP. The second criterion of Koch and Popelier relates ρ_b and ab initio calculated hydrogen bond energy. In our experimental studies, we apply the above expression for the potential energy density $V(r_{CP})$ at BCPs, which can be taken to be proportional to the hydrogen bond energy (Figure 6).[46]

(59) Pauling, L. *The Nature of the Chemical Bond*; Cornell University Press: Ithaca, New York, 1960.

Although a linear relationship between $V(r_{CP})$ and ρ_b could be fitted with correlation coefficient $R = -0.99$, the linear model needs to be extended because of non random distribution of the residuals around the regression line. This distribution seems to suggest a quadratic term as a possible extension of the linear model. Again, this small departure from the linearity of the model results from the broad range of interactions analyzed. It is the strongest and weakest interactions which cause the deviation from linearity.

As one can see, all data points for the weakest C−H···O interactions are clustered at one end of the plot. In fact, the slope of the linear dependence for these interactions is equal to −241(15) and it differs significantly from the linear part of the quadratic relation.

Additionally, there exist strong relationships between the local energy densities and the length of the interaction lines (see Figure 7). These relationships have similar features as the dependence of ρ_b on R_{ij}.

These dependences of the local kinetic and potential energy densities parallel the relationships found by Espinosa et al.[46] for energies calculated from topological and structural data for a set of 83 accurate electron density studies involving X−H···O (X = C, N, O) hydrogen bonds. The parameters of the exponential functions fitted to the data in Figure 7 differ significantly from those found by Espinosa et al. This is probably accounted for by the wider range of types of interactions present in our study.

The third criterion enumerated by Koch and Popelier[43] relates to $\nabla^2\rho_b$ which as they specified should have positive values, i.e., interactions should be of ionic type. The distribution of the experimental values of $\nabla^2\rho_b$ for all interactions is shown in Figure 8.

The range of $\nabla^2\rho_b$ encompasses both positive and negative numerical values, which can be seen to have a quantitative meaning. There is in fact a continuous dependence of $\nabla^2\rho_b$ on R_{ij} (see Figure 8). The plot can be divided into sections corresponding to different sub-ranges of R_{ij}. For $R_{ij} < 1.6$ Å, $\nabla^2\rho_b$ has negative or small positive values typical of covalent bonds. When $\nabla^2\rho_b = 0$, R_{ij} equals ca. 1.3 Å which corresponds to the limit of covalent bonds discussed in the context of Figure 5. Espinosa et al.[46,49,51] pointed out that this distance corresponds to the boundary between shared and closed shell interactions. For 1.3 Å $< R_{ij} <$ 2.1 Å, there is a transition from covalent to ionic type of interactions in which the slope of the $\nabla^2\rho_b$ curve changes from positive to negative, with the maximum at $R_{ij} =$ ca. 1.6 Å. For $R_{ij} > 2.1$ Å, $\nabla^2\rho_b$ has values typical of weak ionic interactions, i.e., hydrogen bonds. The close fit of a Morse function to the distribution of $\nabla^2\rho_b$ is particularly striking. Espinosa et al. in their studies using both experimental (for X−H···O interactions)[49] and ab initio calculated (for X−H···F interactions)[51] topological data also observed Morse-type dependences. They have even retrieved interaction potentials from the topology of the electron density[48] and pointed out that Buckingham and Matsuoka−Clementi−Yoshimin potentials can also be fitted to their data. In a very recent paper,[51] they present a conclusion, based on calculated data for X−H···F interactions, consistent with ours, namely that there is a continuum of properties encompassing the whole range from weak to strong interactions.

(60) Abramov, Yu. A. *Acta Cryst* **1997**, *A53*, 264−272.

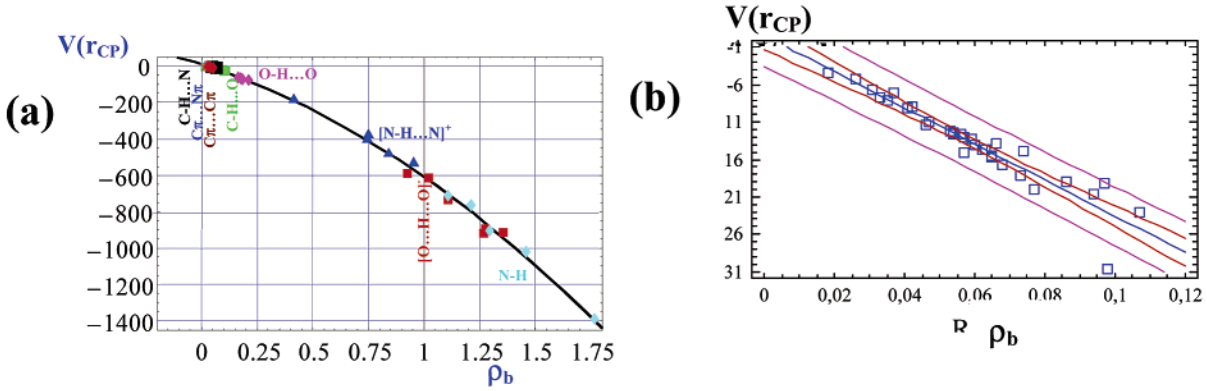

Figure 6. Results of fitting quadratic and linear models to describe the relationship between local potential energy density $V(r_{CP})$ [kJ mol^{-1}bohr^{-3}] and ρ_b [eÅ^{-3}]: (a) general dependence for all data points $V(r_{CP}) = 10(3) - 390(17)\rho_b - 230(12)\rho_b^2$, $N = 63$, $R = -0.99$; (b) the dependence for C−H···O interactions: $V(r_{CP}) = 0.6(9) - 241(15)\rho_b$, $R = -0.95$ for $N = 33$ data points, confidence and tolerance intervals at $\alpha = 0.05$ significance level.

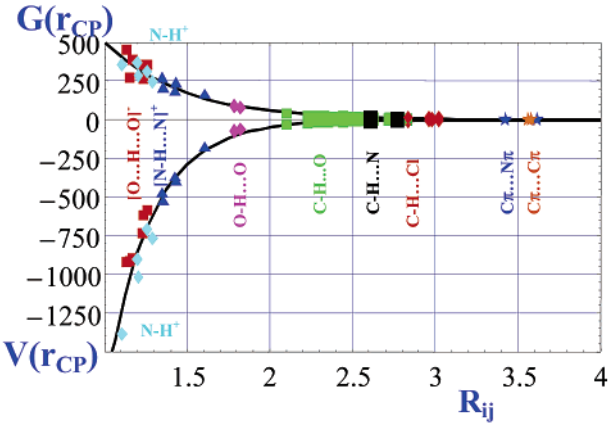

Figure 7. Results of fitting exponential models describing relationships between: $V(r_{CP})$ [kJ mol^{-1}bohr^{-3}] and R_{ij} [Å]for H···X: $V(r_{CP}) = -3(9) - \exp[11.1(3) - 3.7(2)R_{ij}]$, $N = 63$, $R = 0.99$; $G(r_{CP})$ [kJ mol^{-1} bohr^{-3}] and R_{ij} [Å]: $G(r_{CP}) = 3(7) + \exp[(8.4(2) - 2.1(2)R_{ij}]$, $N = 63$, $R = 0.98$.

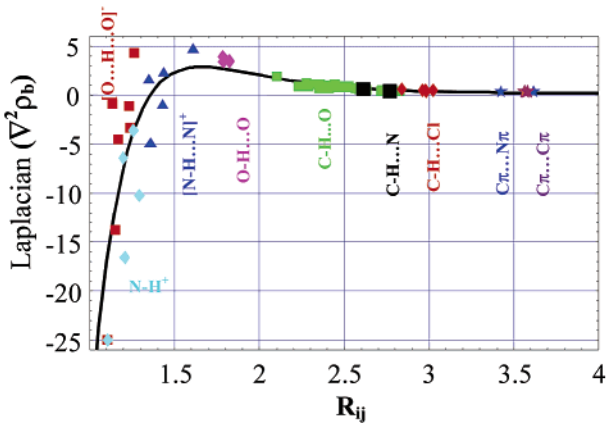

Figure 8. Morse type dependence of $\nabla^2\rho_b$ [eÅ^{-5}] on the length of interaction line [Å]: $\nabla^2\rho_b = 3(1) - 3(2)\{1 - \exp[-2.3(6)(R_{ij} - 1.66(8))]\}^2$, curvilinear correlation coefficient $R = 0.78$ for $N = 63$ datapoints.

The fourth criterion of Koch and Popelier[43] concerns the mutual penetrations of the donor and acceptor atoms. The nonbonded radii r_D° and r_A° of the donor and acceptor atoms are compared with their corresponding bonding radii (r_D and r_A). The quantity $\Delta r_D + \Delta r_A$ represents the interpenetration of van der Waals spheres of the donor and acceptor atoms. It appears that there is a strong linear correlation between $\Delta r_D + \Delta r_A$ and R_{ij} (see Figure 9).

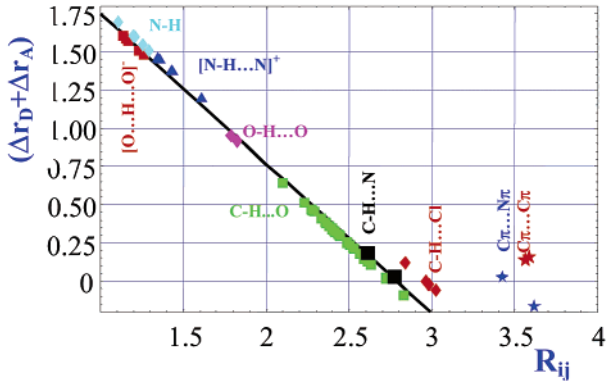

Figure 9. Linear dependence of $(\Delta r_D + \Delta r_A)$ [Å] on R_{ij} [Å]: $(\Delta r_D + \Delta r_A) = 2.72(3) - 0.98(1)R_{ij}$, $N = 63$, $R = -0.99$. $\pi...\pi$ interactions deviate from the regression line.

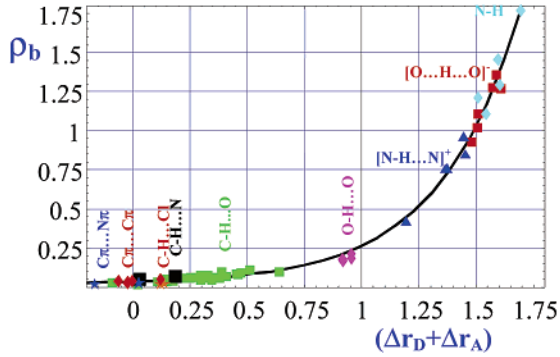

Figure 10. Exponential dependence of ρ_b on $(\Delta r_D + \Delta r_A)$ (a) for all interactions $\rho_b = 0.021(8) + \exp[-4.2(2) + 2.8(1)(\Delta r_D + \Delta r_A)]$, $N = 63$, $R = 0.99$; for subset C−H···O hydrogen bonds there is a linear dependence of ρ_b on $(\Delta r_H + \Delta r_O)$: $\rho_b = 0.025(4) + 0.12(1)(\Delta r_H + \Delta r_O)]$, $N = 33$, $R = 0.88$.

The negative values of $\Delta r_D + \Delta r_A$ correspond to cases where the van der Waals spheres do not intersect, and therefore the Koch and Popelier fourth criterion is not fulfilled and these cases cannot be considered as hydrogen bonds, even though they follow the overall dependence of $\Delta r_D + \Delta r_A$ on R_{ij}. There is also a group of points which do not follow the same dependence and these are found to correspond to some $\pi\cdots\pi$ interactions.

$\Delta r_D + \Delta r_A$ also correlates with ρ_b (Figure 10). In general, there is an exponential dependence, although it is linear when only C−H···O interactions are considered. Overall the highest

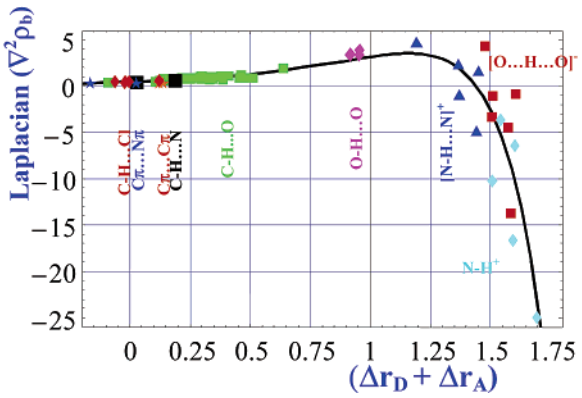

Figure 11. Morse type dependence of $\nabla^2\rho_b$ [eÅ^{-5}] on interpenetration parameter ($\Delta r_D + \Delta r_A$) [Å]: $\nabla^2\rho_b = 3.5(9) - 3.4(1.5)\{1 - \exp[2.5(4)\text{-}(1.16(4) - (\Delta r_D + \Delta r_A))]\}^2$, $R = 0.87$ for $N = 63$ data points.

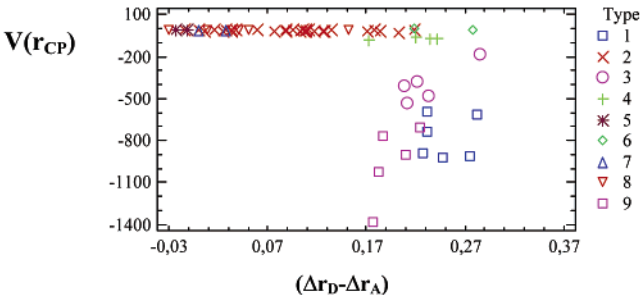

Figure 12. Dependence of $V(r_{CP})$ [kJ mol^{-1}bohr^{-3}] on the ($\Delta r_D - \Delta r_A$) [Å] interpenetration parameter. The code for the type of interactions is as follows: (1) [O···H···O]$^-$, (2) C−H···O, (3) [N−H···N]$^+$, (4) O−H···O, (5) C−H···N, (6) Cπ···Nπ, (7) Cπ···Cπ, (8) C−H···Cl, and (9) N−H$^+$.

values of ρ_b correspond to the greatest interpenetration of the van der Waals spheres.

The sum ($\Delta r_D + \Delta r_A$) correlates also with $\nabla^2\rho_b$ (Figure 11). There is a Morse type dependence of $\nabla^2\rho_b$ on $\Delta r_D + \Delta r_A$, similarly as for the dependence of $\nabla^2\rho_b$ on R_{ij} (Figure 8).

Here, the greatest interpenetrations correspond to the covalent region of the $\nabla\ ^2\rho_b$ curve. The most positive laplacian values occur when the interpenetration is ca. 1.2 Å.

Finally, we consider the criterion involving $\Delta r_D - \Delta r_A$. Geometrically, this represents the amount by which the critical point penetrates the donor's van der Waals sphere more than the acceptor's van der Waals sphere. This is positive, hence the criterion is fulfilled, for nearly all 63 interactions considered. There is an interesting variation of the local potential energy density with $\Delta r_D - \Delta r_A$ (see Figure 12).

For the weaker type of interactions (all types with exception of [O···H···O]$^-$, [N−H···N]$^+$ and N−H$^+$, $V(r_{CP})$ is almost constant. For the strongest bonds however, the potential energy tends to have by far larger values and the critical points penetrate the donor's van der Waals sphere considerably more than the acceptor's, although there is no systematic dependence of $V(r_{CP})$ on $\Delta r_D - \Delta r_A$ in this region.

It should be noted that even the weakest interactions, with a very few exceptions, in the above analyses do in fact fulfill the interpenetration criteria of Koch and Popelier and therefore do not simply represent nonbonding, short contacts imposed by stronger interactions. It is interesting to note that $V(r_{CP})$ for the cases of negative $\Delta r_D - \Delta r_A$ values lies on the same line as for the interactions with positive $\Delta r_D - \Delta r_A$. This is a consequence of both $V(r_{CP})$ and $G(r_{CP})$ being close to zero for the weakest types of interactions.

Role of a Minor Secondary [Me$_2$N−H···NMe$_2$]$^+$···X$^{\delta-}$ Interaction. The crystal structures of the complexes **DMANH$^+$ A$^-$** are either built up from layers of pairs of stacked cations and anions which form molecular planes, or from one single **DMANH$^+$** cation (anion) interacting with six anions (cations) in the closest 3D neighborhood. This resembles the type of close packing characteristic for ionic inorganic compounds. In the first case, two cations and two anions are placed in an antiparallel manner due to strong dipole−dipole interactions and other kinds of weak interactions discussed above.

Many of the C−H···Acceptor hydrogen bonds involve methyl hydrogen atoms of the DMANH$^+$ cations. When one considers a slightly larger fragment than just the three atoms [N−H···N]$^+$ participating in the strong, electrostatic hydrogen bond, it is apparent that this bond has a multicenter character which can be represented by the formula of [Me$_2$N−H···NMe$_2$]$^+$···X$^{\delta-}$, where X is the nearest electronegative atom (usually oxygen) in the crystal lattice. The detailed consequences of this arrangement will be the subject of a subsequent paper.

Conclusions

At the level of molecular geometry, the **DMANH$^+$** cations in the four complexes studied show consistent effects of asymmetric protonation. The topological properties of the covalent bonds in the cations generally reflect the trends in geometry.

In the four crystal structures there exist networks of interactions of varying strength, which are classified into nine types. When these are taken together with previously published results for the complex of DMAN with dichloromaleic acid a total of 63 interactions can be identified. The lengths of the interaction lines can be correlated with topological properties, local kinetic and potential energy densities, interpenetrations of van der Waals spheres, and interpenetrations of CPs with van der Waals spheres. When the full range of interactions including the N−H$^+$ covalent bonds is considered, the variation of the laplacian of ρ at BCPs reveals a continuous transition from the weak hydrogen bonding to the covalent bonding situation. It appears that quantitative relationships or unifying dependencies exist, derived from charge density distributions, linking weak π···π electron interactions, weak and strong hydrogen bonds, and covalent bonds. These general relationships open a new field which can be termed "quantitative crystal engineering". With the development of supramolecular chemistry toward designed materials and molecular machines, the potential importance of such information for fine-tuning intermolecular interactions seems highly significant.

Even the weakest interactions, with two exceptions, present in the crystal structures studied do in fact fulfill the interpenetration criteria of Koch and Popelier and therefore do not simply represent nonbonding, short contacts imposed by stronger interactions.The strong, charge-supported intramolecular [N−H···N]$^+$ hydrogen bond has a multicenter character which can be represented by the formula {[Me$_2$N−H···NMe$_2$]$^+$··· X$^{\delta-}$}, where X is the nearest electronegative atom in the crystal lattice.

Acknowledgment. Beam time allocation by ISIS under RB/6765 SXD is gratefully acknowledged. We also thank the UK

EPSRC for a fellowship (GR/M90382) for G.T.S. and the Royal Society, the Polish Academy of Sciences, and the University of Warsaw for enabling P.R.M. and K.W. to participate in the European Science Exchange Programme.

Supporting Information Available: Fractional atomic coordinates and anisotropic displacement parameters, monopole charges, κ' and κ'' values obtained from the refinement, critical point data, multipole population coefficients, definitions of local axes, bond lengths and angles for all the **DMAN**H^+ complexes studied in this paper. This material is available free of charge via the Internet at http://pubs.acs.org.

JA029389B